Available online at www.sciencedirect.com
ScienceDirect
Combustion and Flame 155 (2008) 358–368
Combustion and Flame
www.elsevier.com/locate/combustflame

Measurements of laminar burning velocities and Markstein lengths for methanol–air–nitrogen mixtures at elevated pressures and temperatures

Zhiyuan Zhang, Zuohua Huang *, Xiangang Wang, Jun Xiang, Xibin Wang, Haiyan Miao

State Key Laboratory of Multiphase Flow in Power Engineering, Xi'an Jiaotong University, Xi'an, People's Republic of China

Received 25 January 2008; received in revised form 4 July 2008; accepted 22 July 2008

Abstract

The laminar burning velocities and Markstein lengths for the methanol–air mixtures were measured at different equivalence ratios, elevated initial pressures and temperatures, and dilution ratios by using a constant volume combustion chamber and high-speed schlieren photography system. The influences of these parameters on the laminar burning velocity and Markstein length were analyzed. The results show that the laminar burning velocity of the methanol–air mixture decreases with an increase in initial pressure and increases with an increase in initial temperature. The Markstein length decreases with an increase in initial pressure and initial temperature, and increases with an increase in the dilution ratio. A cellular flame structure is observed at an early stage of flame propagation. The transition point is identified on the curve of flame propagation speed against stretch rate. The reasons for the cellular structure development are also analyzed.

Keywords: Methanol; Laminar burning velocity; Markstein length; Flame stability

1. Introduction

Due to the limited crude oil reserves, the investigation on alternative fuels has attracted more attention in recent years. For spark ignition engines, the alternative fuels include methanol, ethanol, compressed natural gas (CNG) and liquid petroleum gas (LPG). Sources of methanol are potentially abundant at an acceptable price. Compared with gasoline, the regulated emissions with methanol are usually lower than from engines fueled with pure methanol or gasoline–methanol blends. Until now, many studies have been conducted on the applications of methanol in internal combustion engines. Most work has concentrated on the combustion and emission characteristics of these fuels in engines [1,2], with less emphasis on their fundamental combustion characteristics, such as laminar burning velocity, Markstein length, flammability limits, and flame front instabilities. These fundamental combustion characteristics of methanol are necessary for deepening our understanding of engine combustion processes and this is the motivation for the present study.

* Corresponding author at: School of Energy and Power Engineering, Xi'an Jiaotong University, Xi'an 710049, People's Republic of China.
E-mail address: zhhuang@mail.xjtu.edu.cn (Z. Huang).

0010-2180/$ – see front matter
doi:10.1016/j.combustflame.2008.07.005

Laminar burning velocity is a fundamental parameter of laminar premixed flames and can be used to validate the chemical kinetic mechanism. It provides basic data also for turbulent combustion. Previous studies have measured the laminar burning velocity of hydrogen–air, iso-octane–air and natural gas–hydrogen–air mixtures [3–6]. Various methods have been employed involving stationary flames (counterflow double flames [7]) and non-stationary flames (outwardly-propagating spherical flames [8]). The counterflow double flames are convenient for measuring laminar burning velocity of both liquid and gaseous fuels with easy controlling mixture compositions, but this method is usually limited to atmospheric pressure and room temperature. It is difficult to use it for measurements at the elevated pressures and the flame stretch rate must be measured [9]. For spherically expanding flames, the stretch imposed on the premixed flames is well defined and asymptotic theories and measurements suggest a linear relationship between flame speeds and flame stretch rate. In addition, other laminar combustion properties, such as Markstein lengths (or Markstein numbers), can be obtained simultaneously from spherically expanding flames. Markstein lengths characterize the variation in the local flame speed with stretch rate, they can also characterize flame instabilities and the stretch rates for flame quenching. For these reasons, the spherically expanding flame has been widely used to determine the unstretched laminar burning velocities [10,11]. In this study, the outwardly-propagation spherical flame was used to measure the laminar burning velocity of the premixed methanol–air mixtures.

For gaseous fuels, such as methane and hydrogen [3,5,6,8,12], homogeneous fuel–air mixtures are easily prepared. Some researches have reported the premixed laminar combustion characteristics of the liquid fuels like methanol, ethanol and gasoline. Metghalchi and Keck [13], Gülder [14], Saeed and Stone [9] have measured laminar burning velocities of methanol–air mixtures using closed combustion chambers, and have computed values based on combustion models and pressure–time data. However, their studies did not report the effect of flame stretch on the flame propagation speed or analyse the cellular flame structure. Consequently their method may lead to an overestimation of the laminar burning velocity. Liao et al. [15] provided the laminar burning velocity of the methanol–air mixtures at atmospheric pressure and relatively low temperature using a constant volume combustion chamber and high-speed schlieren photography. The purpose of this study is to remedy a dearth of data by measuring the laminar burning characteristics of methanol–air mixtures at elevated pressures and temperatures, over a wide range of equivalence ratios, and with nitrogen as a diluent. Flame front instabilities and cellular flame structure are also discussed.

2. Experimental apparatus and procedures

Fig. 1 shows the experimental arrangement. This includes a constant volume combustion chamber,

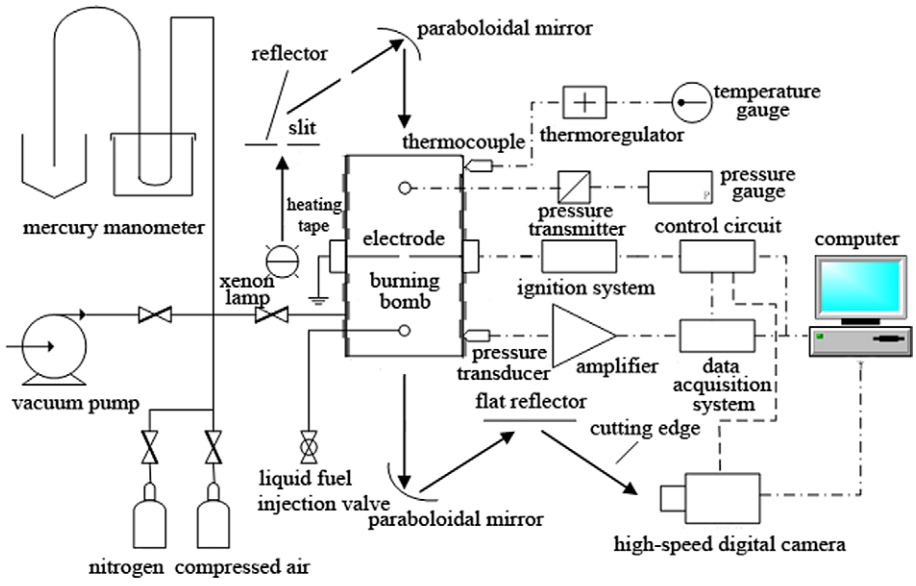

Fig. 1. Experimental arrangement.

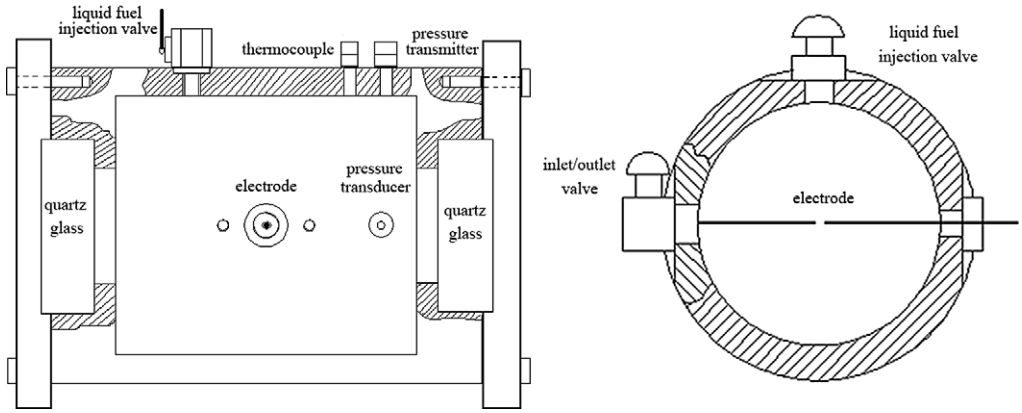

Fig. 2. Constant volume combustion chamber.

and systems for heating, ignition, data acquisition and high-speed schlieren photography. The combustion chamber is a cylinder with an inner diameter of 180 mm and volume of 5.5 liter as shown in Fig. 2. The centrally located electrodes ignite the combustible mixture. The pressure transmitter, thermocouple, pressure transducer, liquid fuel injection valve, inlet and outlet valves are mounted on the chamber body. Two quartz windows of 80 mm diameter are mounted on the two sides of the vessel. A high-speed digital camera (HG-100K) operating at 10,000 frames per second recorded the flame progression during the combustion. The partial pressures of each component are regulated by a mercury manometer when the initial pressure of the mixtures in the vessel is less than or equal to 0.1 MPa. The partial pressures are regulated by the pressure transmitter at initial pressures greater than 0.1 MPa. The entire vessel was heated by a 2.4 kW heating-tape wrapped outside the chamber body. The thermocouple measures the initial temperature of mixtures in the vessel to an accuracy of 1 K. The initial temperature is adjusted by a thermo-regulator. When the mixture reaches the designated initial temperature, the power is switched off. The required liquid fuel is injected into the chamber corresponding to the given initial temperature, initial pressure, equivalence ratio and dilution ratio. Bomb dry air and diluent are supplied into the chamber through the inlet/outlet valve. A time of 5 to 10 min elapsed before ignition.

The equivalence ratios ranges from 0.7 to 1.8, nitrogen dilution ratios are 0.05, 0.1 and 0.15, initial temperatures are 373 K, 423 K and 473 K, and initial pressures are 0.1 MPa, 0.5 MPa and 0.75 MPa. Dilution ratio ϕ_r is defined as the ratio of the dilution gas partial pressure to that of the total mixture,

$$\phi_r = \frac{p_{\text{diluent}}}{p_{\text{diluent}} + p_{\text{air}} + p_{\text{fuel}}}, \tag{1}$$

where P_{air}, P_{fuel} and P_{diluent} are the partial pressures for air, vaporized fuel and diluent, respectively.

3. Laminar burning velocity and Markstein length

For a outwardly-propagating spherical flame, the stretched flame velocity, S_n, reflecting the flame propagation speed, is derived from the flame radius versus time:

$$S_n = \frac{dr_u}{dt}, \tag{2}$$

where r_u is the radius of the flame in Schlieren photograph and t is the elapsed time from spark ignition.

A general definition of stretch at any point on the flame surface is the Lagrangian time derivative of the logarithm of the area A of any infinitesimal element of the surface:

$$\alpha = \frac{d(\ln A)}{dt} = \frac{1}{A}\frac{dA}{dt}. \tag{3}$$

For the outwardly-propagating spherical flame, the flame stretch rate can be simplified as,

$$\alpha = \frac{1}{A}\frac{dA}{dt} = \frac{2}{r_u}\frac{dr_u}{dt} = \frac{2}{r_u}S_n. \tag{4}$$

In respect to the early stage of flame expansion, there exists a linear relationship between the flame speeds and the flame stretch rate [8]; that is,

$$S_l - S_n = L_b\alpha, \tag{5}$$

where S_l is the unstretched flame propagation speed, which is obtained as the intercept value of S_n at $\alpha = 0$ in the plot of S_n against α. Burnt-gas Markstein length L_b is the slope of S_n vs. α curve. The diffusional-thermal instability of the flame front is dependent upon L_b. Positive values of L_b, which correspond to Lewis numbers larger than unity, and that the

flame speed decreases with the increase of the stretch rate. A negative value of L_b corresponds to a Lewis number smaller than unity, indicating that the flame speed increases with the increase of flame stretch rate. Negative values of L_b are associated with more unstable flames [6,16,17].

The characteristics of the igniter can influence the measured value of burning velocity. Previous study showed that the flame speeds were independent of ignition energy when flame radius is greater than 6 mm [6]. This phenomenon was also observed by Bradley et al. [4], Lamoureux et al. [11] and Liao et al. [15]. Their studies gave the value approximately to 6 mm so as to avoid possible effect caused by the spark ignition disturbance completely. When the flame radii is smaller than 25 mm, the pressure in the constant volume combustion chamber varies little to ensure the combustion process to be a constant-pressure one. Considering both avoiding the effect of ignition energy and pressure rise, the flame photos during the range of 6 mm to 25 mm are used in the analysis. In addition, the measurements were also restricted by the occurrence of the cellular structure due to the obvious increasing of flame speed by the increased flame front area [4,9,16].

If the rate of change of pressure is negligible, a simple relationship links the unstretched flame speed S_l and unstretched laminar burning velocity u_l is given as,

$$u_l = \rho_b S_l / \rho_u, \tag{6}$$

where ρ_b and ρ_u are the densities for burned gases and unburned gases.

Due to the finite flame thickness, there exist two possible definitions for the stretched laminar burning velocity depending on whether the burning velocity is defined at the unburned gas side or burned gas side. These two burning velocities, which are proposed by Bradley et al. [4,12], are the stretched laminar burning velocity u_n and the stretched mass burning velocity u_{nr}, respectively. Stretched laminar burning velocity u_n and the stretched mass burning velocity u_{nr} are calculated by:

$$u_n = S\left[S_n \frac{\rho_b}{\rho_u}\right], \tag{7}$$

$$u_{nr} = \frac{\rho_b}{\rho_b - \rho_u}(u_n - S_n), \tag{8}$$

where S is a function that depends upon the flame radius and density ratio [12]. It accounts for the effect of the flame thickness on the mean density of the burned gases. The expression of S in the study used the formula given by Bradley et al. [4],

$$S = 1 + 1.2\left[\frac{\delta_l}{r_u}\left(\frac{\rho_u}{\rho_b}\right)^{2.2}\right] - 0.15\left[\frac{\delta_l}{r_u}\left(\frac{\rho_u}{\rho_b}\right)^{2.2}\right]^2. \tag{9}$$

Here δ is the laminar flame thickness, given by $\delta_l = \nu/u_l$, in which ν is the kinetic viscosity of the unburned mixtures.

The flame thickness gives rise to the difference between the stretched laminar burning velocity u_n and the stretched mass burning velocity u_{nr}. The difference between u_n and u_{nr} is most marked during the early stage of flame propagation when the flame front is relatively thick.

4. Results and discussions

4.1. Flame propagation speeds and Markstein length

Fig. 3 shows the schlieren photographs of the methanol–air flames at an equivalence ratio, ϕ, of 1.0, initial temperature of 373 K and initial pressure of 0.1 MPa. In this case, the smooth spherically expanding flame propagates from the chamber center. At the early stage of flame development, the cooling effect of the electrodes on the flame propagation is observed and this leads to slow flame propagation along the direction of the electrodes comparing with the vertical direction. When the flame radius has developed to a certain value, there is little effect of the electrodes. To avoid the influence from the electrodes, the flame radius used in the calculation uses the radius in the vertical direction.

Fig. 4 plots the flame radius versus the time for methanol–air mixtures at three different ϕ. In the early stage of flame development, the effects of ignition energy and electrode cooling can be observed. Fig. 5 shows the stretched flame propagation speed

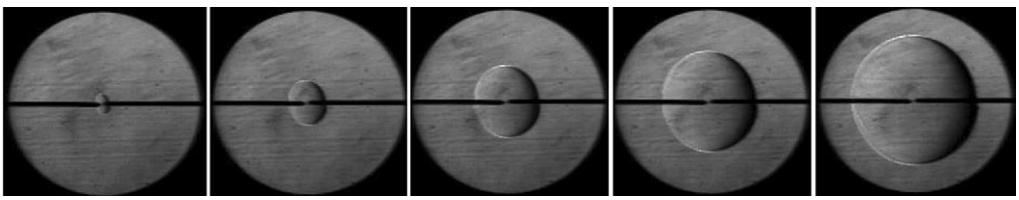

Fig. 3. Schlieren photographs of methanol–air mixtures.

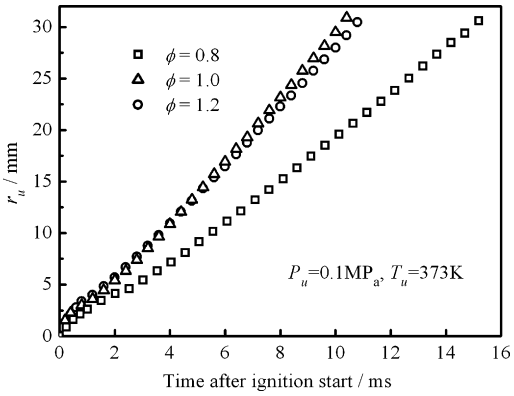

Fig. 4. Flame radius versus time at various equivalence ratios.

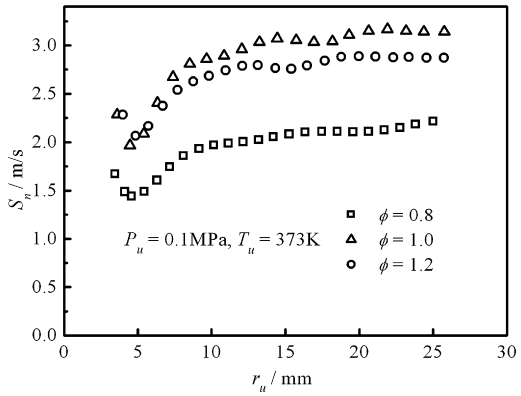

Fig. 5. Stretched flame speeds versus flame radius.

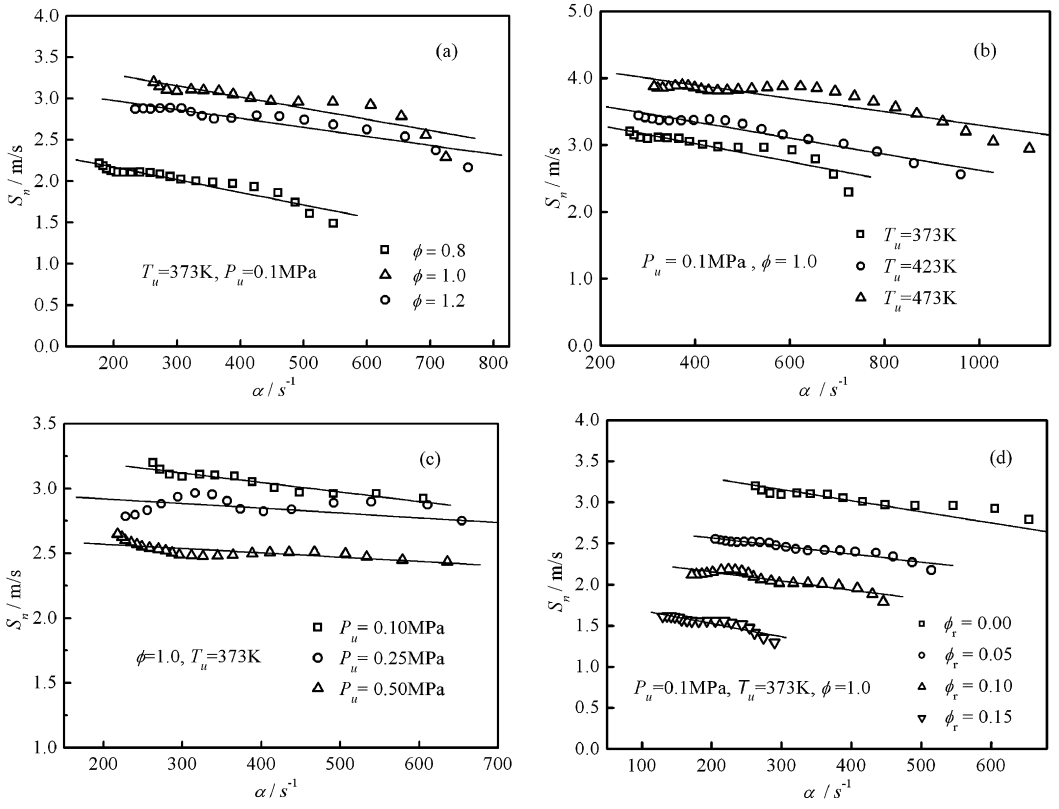

Fig. 6. Stretched flame speed versus the stretch rate.

versus the flame radius at three equivalence ratios, initial temperature of 373 K and initial pressure of 0.1 MPa. The flame propagation speed increases gradually with increase in spherical flame radius. In the early stage of flame development, the flame propagation speeds give a decreasing trend and then changes to an increasing trend with the increase of flame radius. This phenomenon reveals that flame stretch can be more important on flame propagation. The stretched flame speeds show an increase with the increase of initial temperature and a decrease with the increase of initial pressure and dilution ratio. Mixture dilution will reduce the chance for fuel–oxygen combination and decreases the temperature as diluent absorbs some of the released heat, resulting in the decrease of flame propagation speed.

Fig. 6 shows stretched flame speeds versus flame stretch rate at different equivalence ratios, initial tem-

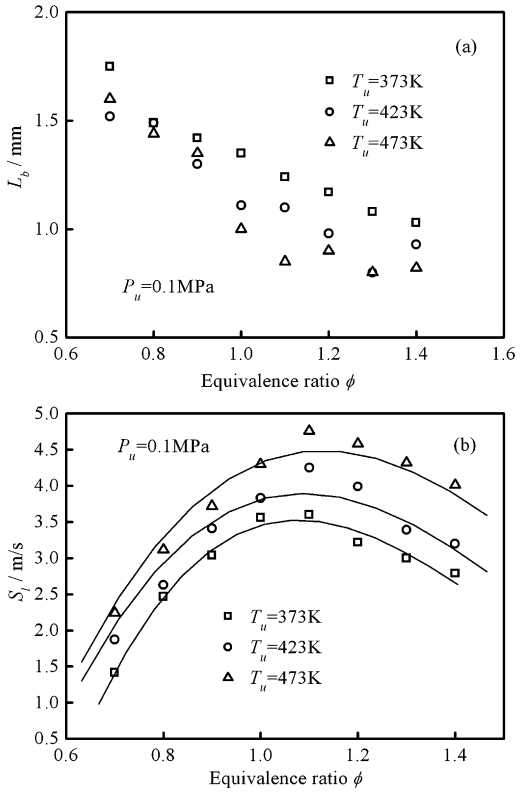

Fig. 7. Unstretched flame speed and Markstein length at different initial temperatures.

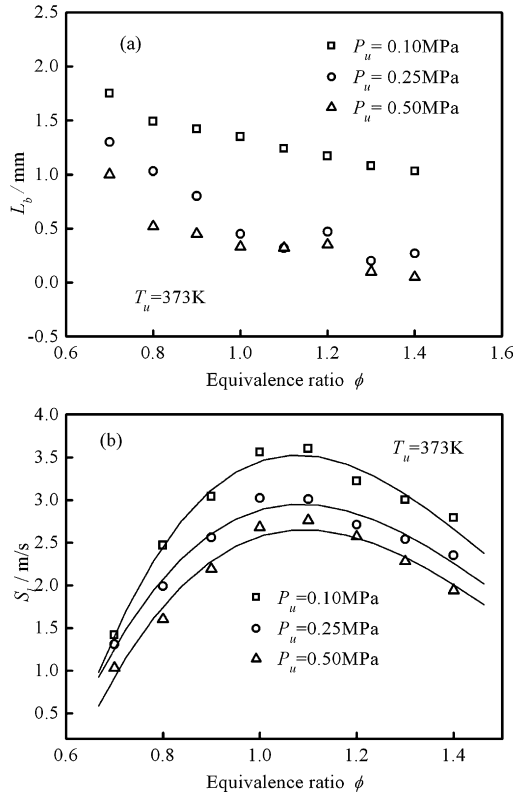

Fig. 8. Unstretched flame speed and Markstein length at different initial pressures.

peratures, initial pressures and dilution ratios. In the early stage of the flame propagation when the flame radius is small, the stretch rate of flame front surface is large and the flame propagation speed gives a low value. As the flame propagates outwardly, the flame stretch rate is decreased and flame propagation speed is increased. Removing the data affected by ignition energy and electrodes during the early stage of flame development gives a linear correlation line for the stretched flame speed and the flame stretch rate as shown in the figure. The unstretched flame propagation speed is obtained as the intercept value of S_n at $\alpha = 0$ in the plot of S_n vs. α. Importantly, this gives the value of laminar burning velocity u_l from Eq. (6). For all cease in the study, the gradients of the lines take the negative value, corresponding to a positive value of Markstein length.

In the case of methanol–air–diluent mixture combustion, dilution will decrease the flame propagation speed, thus the flame stretch rate has the low value with the increase of dilution ratio at the same flame radius, and the data of S_n concentrates into a narrow range of stretch rate while increasing the dilution ratio.

Fig. 7 gives the Markstein lengths (L_b) and unstretched flame propagation speeds (S_l) versus the equivalence ratios. The Markstein length decreases monotonously with increase in equivalence ratio and decreases with the increase of initial temperature. This suggests that rich mixtures and/or high initial temperature will lead to instability of the flame front. The diffusively-thermal stability of lean methanol–air mixtures is stronger than that of rich mixtures. The occurrence of wrinkled and cellular flame structure develops more readily with rich mixtures and high initial temperature. The unstretched flame propagation speed increases with the increase of the initial temperature due to enhanced chemical reaction rate. The peak value of the unstretched flame propagation speed occurs at an equivalence ratio slightly larger than unity and the position of the peak value shifts to the richer mixture side as the initial temperature increases.

Fig. 8 illustrates the variation of Markstein lengths and unstretched flame propagation speeds with ϕ at different initial pressures. The Markstein length decreases with the increase of the initial pressure, as does the unstretched flame speed. This indicates that flame stability decreases with the increase of the initial pressure. The peak values of the unstretched flame propagation speed occur with ϕ slightly larger than unity and show little variation with initial pressure.

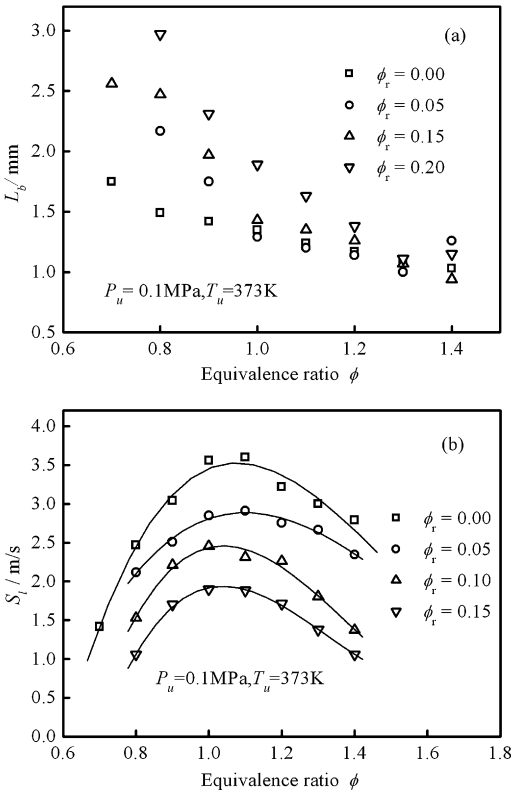

Fig. 9. Unstretched flame speed and Markstein length at different gas dilution ratios.

The Markstein lengths and unstretched flame propagation speeds versus the equivalence ratio at different dilution ratios are demonstrated in Fig. 9. The Markstein length increases with the increase of the dilution ratio. This suggests that addition of diluent into the methanol–air mixtures can increase the stability of the flame front. The unstretched flame propagation speed decreases with the increase of the dilution ratio, and the position of the peak value of the unstretched flame propagation speed shows little variation with dilution ratios.

4.2. Flame stability and cellular structure

Fig. 10 shows schlieren images of the flame at a flame radius of 30 mm for different initial pressures and equivalence ratios. At the initial pressure of 0.1 MPa, a smooth flame front is observed at three equivalence ratios. When the initial pressure increases to 0.25 MPa, the cellular structure at the flame front begins to occur, especially on the rich mixture side. However, a smooth flame front is retained at small flame radii. When further elevating the initial pressure (0.5 MPa and/or 0.75 MPa), a strong cellular flame front appears at smaller flame radii. For a specific equivalence ratio, the cellular flame structure develops more easily with increase in initial pressure. Fig. 11 shows the detailed development of cellular flame structure with the expansion of the spherical flame at an initial pressure of 0.5 MPa and $\phi = 1.2$. With the expansion of the spherical flame, the cellular structure at the flame front is developed, with the decrease in the local stretch rate. Cellular structure occurs in some positions at a small flame radius and it cracks quickly and develops over the whole surface of the flame front, creating a fully developed cellular structure at larger flame radius. The flame front thickness decreases with the increase of initial pressure, and the hydrodynamic instability is increased as the flame front becomes thinner. These two factors make the early occurrence of the cellular structure for the outwardly-propagating spherical flame with increase of initial pressure. The cellular structure also occurs earlier as the initial temperature is increased. The decrease of Markstein length leads to the decrease of the diffusional-thermal stability, and the results are similar to those from Saeed et al. [9] and Bradley et al. [17]. In the case of cellular flame front, the interface between the unburned mixture and the burned mixture will increases significantly, and this increases the flame propagation speed. To eliminate the acceleration effect in the presence of the cellular structure on the flame propagation speed, flame radii should be limited to radii before the occurrence of cellular structure.

For a clear illustration of the effect of the cellular structure on the flame propagation speed, Fig. 12 plots the flame speed against the stretch rate. There is a rapid increase in S_n at large flame radii (corresponding to the small stretch rate). This transition point marks the onset of the cellular structure. The critical radius corresponds to the second Peclet number, which is defined by Bradley et al. [17]. There is transition point at an initial pressure of 0.1 MPa, but it clearly occurs at an initial pressure of 0.5 MPa or higher for the stoichiometric methanol–air mixture. In the case of initial pressure of 0.75 MPa, with $\phi = 1.0$ and 1.2 there is a clear transition to a cellular structure. The information revealed from the S_n vs. α curve is consistent with the photo observation.

4.3. Laminar burning velocity

Fig. 13 gives the stretched laminar burning velocity u_n and the stretched mass burning velocity u_{nr} versus the stretch rate at different equivalence ratios, initial temperatures, initial pressures and dilution ratios, respectively. In all cases, the stretched laminar burning velocity increases with the increase of the stretch rate, while the mass burning velocity decreases. The difference between the stretched laminar

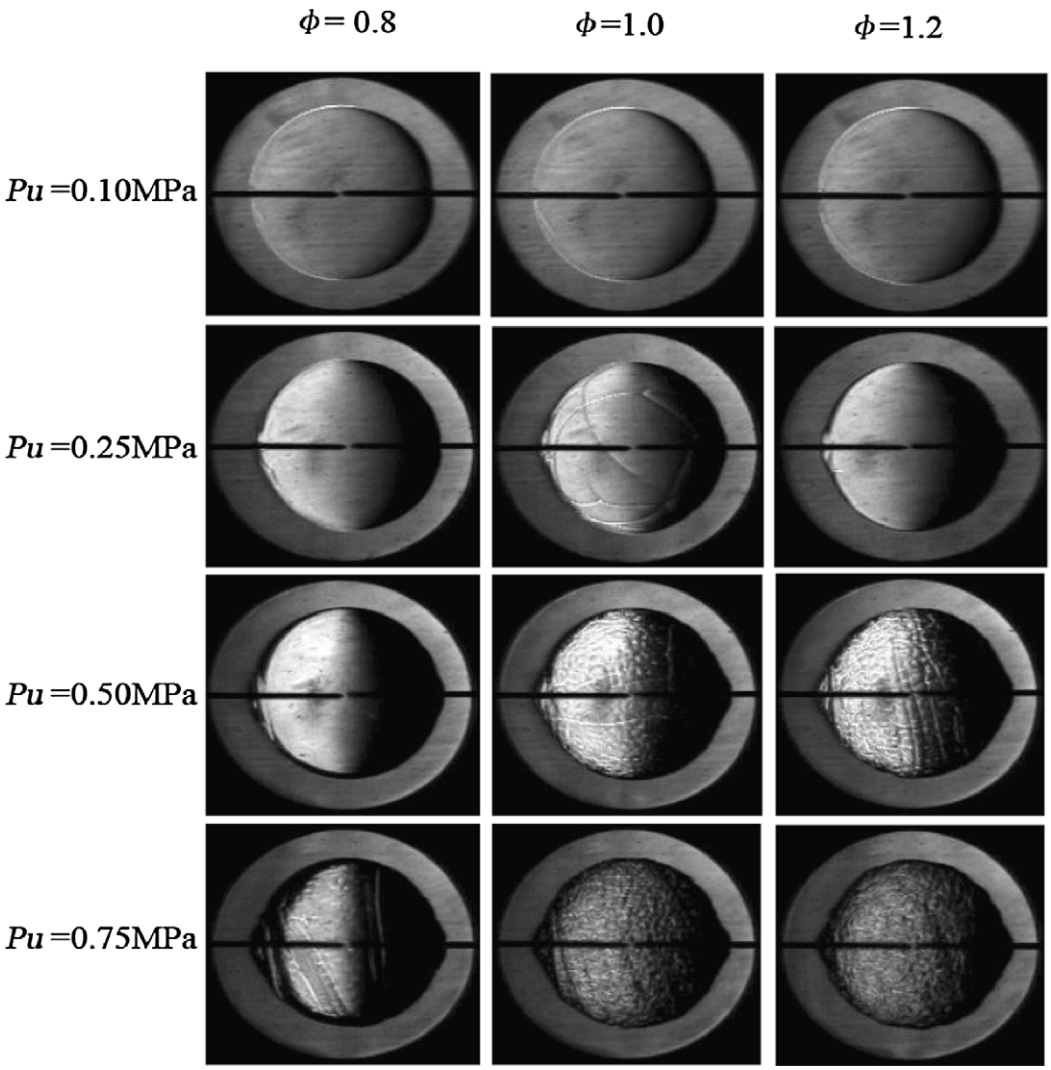

Fig. 10. Schlieren images of laminar flame front at flame radius of 30 mm for different initial pressures and equivalence ratios.

burning velocity and the stretched mass burning velocity can be clearly observed. The stretched laminar burning velocity, which denotes the rate of mixture entrainment, always increases as the stretch rate increases. In contrast, the mass burning velocity, which is the burning velocity related to the production of burned gases, is usually decreased as the stretch rate increases. The difference $(u_n - u_{nr})$ increases with the increase of the stretch rate and this is attributed to the influence of flame thickness on burning velocities. A large value of $(u_n - u_{nr})$ is seen at small radii corresponding to high stretch rate, where the flame thickness is of the same order as the flame radius.

A high stretch rate corresponds to a small flame radius; thus the influence of flame thickness on the burning velocity becomes great. As the stretch rate tends to zero, the effect of flame thickness on burning velocity can be neglected, and u_n and u_{nr} will attain the same value, u_l, the unstretched laminar burning velocity. As shown in Fig. 13a, the value of $(u_n - u_{nr})$ is small at $\phi = 1.0$ and the initial conditions of 0.1 MPa and 373 K. This indicates that the influence of flame thickness on the burning velocity becomes large. As shown in Fig. 13b, the value of $(u_n - u_{nr})$ is large at the initial temperature of 373 K and it decreases with increase of the initial temperature. The influence of flame thickness on the burning velocity becomes large as the initial temperature decreases. Shown in Fig. 13c is the value of $(u_n - u_{nr})$ which is large at 0.1 MPa, and decreases with the increase of the initial pressure. The

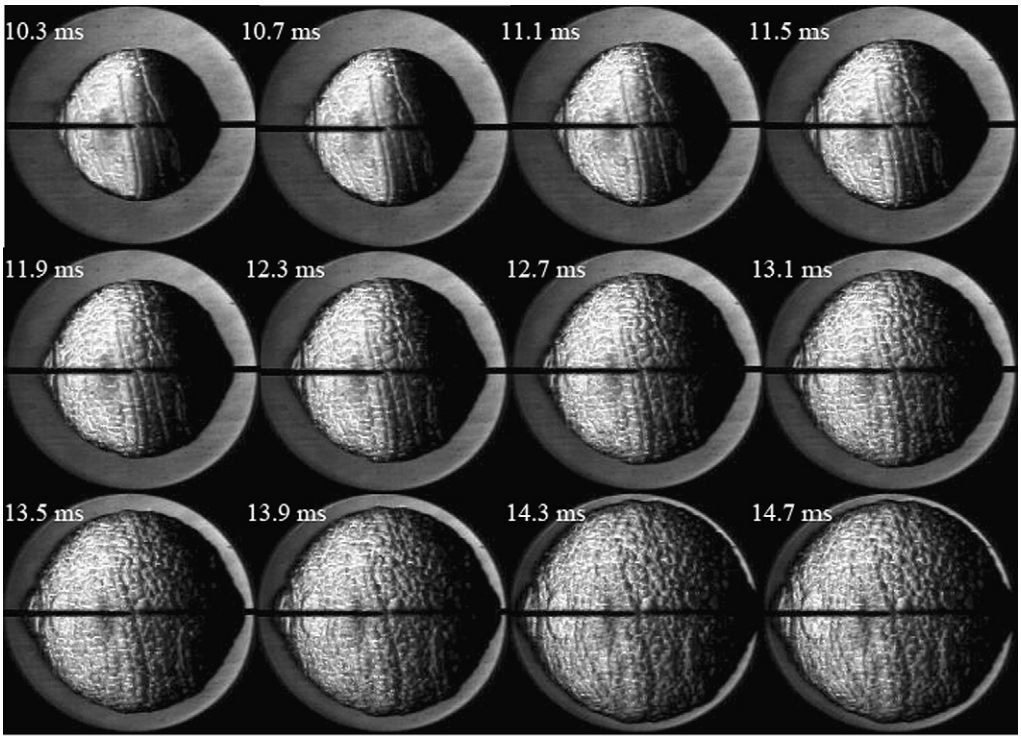

Fig. 11. Development of cellular flame structure with the expansion of the spherical flame.

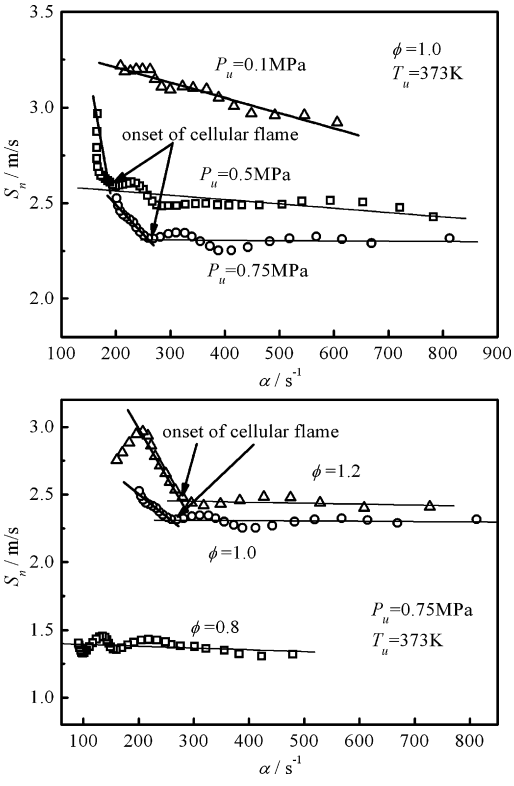

Fig. 12. Stretched flame speed versus the stretch rate.

influence of flame thickness on the burning velocity becomes large as the initial pressure decreases. Shown in Fig. 13d is the value of $(u_n - u_{nr})$ which increases with increase in dilution ratio. This suggests that the influence of flame thickness on the burning velocity becomes large as the dilution ratio increases.

Fig. 14 gives the unstretched laminar burning velocity u_l versus ϕ at different initial temperatures, initial pressures and gas dilution ratios as well as the comparison of the present result with those of other researchers. No data were found for u_l at corresponding elevated temperatures and pressures, and the comparison is limited to room temperature and atmospheric pressure. The literature values of Saeed and Stone [9] and Metghalchi and Keck [13] are recalculated from correlations given in these papers for comparison. The burning velocity decreases with the decrease of the initial temperature and increase in initial pressure. It decreases with increase in dilution ratio. Good agreement is found with the previous studies. The small difference is due to the different in the initial temperature and/or the different method used. Liao at al. [15] took the same method as the present study, thus, the present study gives the best agreement to that reported in [15]. Peak values of the unstretched laminar burning velocities occur at $\phi = 1.1$.

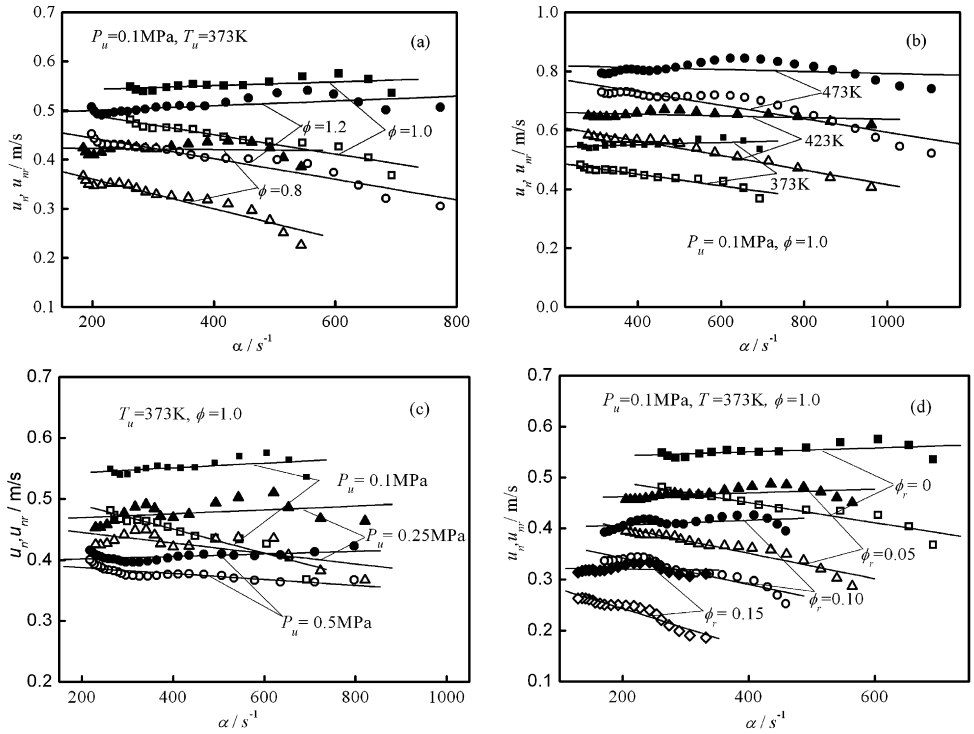

Fig. 13. Stretched laminar burning velocity and stretched mass burning velocity versus stretch rate for different equivalence ratios, initial temperatures and initial pressures, and dilution ratios.

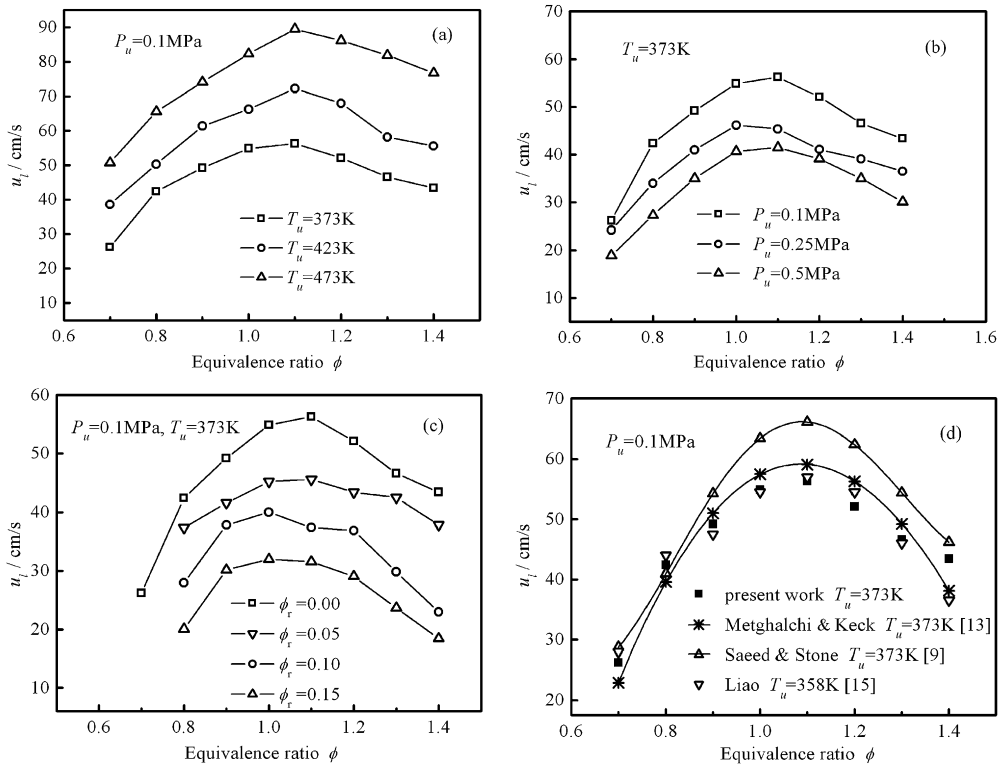

Fig. 14. Unstretched laminar burning velocity versus equivalence ratios.

5. Conclusions

The propagation characteristics of outwardly spherical laminar premixed flame for the methanol–air and methanol–air–diluent mixtures have been studied by a high-speed schlieren photography in a constant volume chamber. The laminar burning velocity and Markstein length at different equivalence ratios, initial pressures and temperature, and dilution ratios are obtained. The main conclusions are:

(1) The flame speed and the laminar burning velocity decrease with the increase of the initial pressure and the dilution ratio, and increases with the increase of the initial temperature. The Markstein length decreases with the increase of equivalence ratios, initial pressures and temperature, and it increases with the increase of dilution ratio.
(2) Flame front instability increases with the increase of equivalence ratio, the initial pressure and temperature. The flame front stability increases with the increase of dilution ratio. The cellular flame structure is presented at the earlier stage with the increase of the initial pressure. The development of cellular flame front increases the flame propagation speed due to the significant increase in the flame front area.
(3) The transition point at S_n vs. α curve is found and this transition point indicates the development of the cellular structure at the flame front. This is consistent to the analysis from the Markstein length and direct image observation.

Acknowledgments

This study was supported by National Natural Science Foundation of China (Nos. 50576070, 50521604).

References

[1] S.H. Liu, C.C.R. Eddy, T.G. Hu, Y.J. Wei, Appl. Therm. Eng. 27 (11–12) (2007) 1904–1910.
[2] M. Abu-Zaid, O. Badran, J. Yamin, Energy Fuels 18 (2) (2004) 312–315.
[3] C.K. Law, O.C. Kwon, Int. J. Hydrogen Energy 29 (8) (2004) 867–879.
[4] D. Bradley, P.A. Hicks, M. Lawes, C.G.W. Sheppard, R. Woolley, Combust. Flame 115 (1–2) (1998) 126–144.
[5] K.T. Aung, M.I. Hassan, G.M. Faeth, Combust. Flame 112 (1–2) (1998) 1–15.
[6] Z. Huang, Y. Zhang, K. Zeng, B. Liu, Q. Wang, D. Jiang, Combust. Flame 146 (1–2) (2006) 302–311.
[7] G. Yu, C.K. Law, C.K. Wu, Combust. Flame 63 (1–2) (1986) 339–347.
[8] X.J. Gu, M.Z. Haq, M. Lawes, R. Woolly, Combust. Flame 121 (1–2) (2000) 41–58.
[9] K. Saeed, C.R. Stone, Combust. Flame 139 (1–2) (2004) 152–165.
[10] S.Y. Liao, D.M. Jiang, J. Gao, Z.H. Huang, Q. Cheng, Fuel 83 (10) (2004) 1281–1288.
[11] N. Lamoureux, N. Djebäýli-Chaumeix, C.E. Paillard, Exp. Therm. Fluid Sci. 27 (4) (2003) 385–393.
[12] D. Bradley, P.H. Gaskell, X.J. Gu, Combust. Flame 104 (1–2) (1996) 176–198.
[13] M. Metghalchi, J.C. Keck, Combust. Flame 48 (1982) 191–210.
[14] O.L. Gülder, Proc. Combust. Inst. 19 (1982) 275–281.
[15] S.Y. Liao, D.M. Jiang, Z.H. Huang, W.D. Shen, C. Yuan, Q. Cheng, Energ. Convers. Manage. 48 (2007) 857–863.
[16] C.K. Law, C.J. Sung, Prog. Energ. Combust. 26 (4–6) (2000) 459–505.
[17] D. Bradley, C.G.W. Sheppard, R. Woolley, D.A. Greenhalgh, R.D. Lockett, Combust. Flame 122 (1–2) (2000) 195–209.